

Downlink and Uplink Intelligent Reflecting Surface Aided Networks: NOMA and OMA

Yanyu Cheng, *Student Member, IEEE*, Kwok Hung Li, *Senior Member, IEEE*, Yuanwei Liu, *Senior Member, IEEE*, Kah Chan Teh, *Senior Member, IEEE*, and H. Vincent Poor, *Life Fellow, IEEE*

Abstract

Intelligent reflecting surfaces (IRSs) are envisioned to provide reconfigurable wireless environments for future communication networks. In this paper, both downlink and uplink IRS-aided non-orthogonal multiple access (NOMA) and orthogonal multiple access (OMA) networks are studied, in which an IRS is deployed to enhance the coverage by assisting a cell-edge user device (UD) to communicate with the base station (BS). To characterize system performance, new channel statistics for the BS-IRS-UD link with Nakagami- m fading are investigated. For each scenario, closed-form expressions for the outage probability and the ergodic rate are derived. To gain further insight, the diversity order and the high signal-to-noise ratio (SNR) slope for each scenario are obtained according to asymptotic approximations in the high-SNR regime. It is demonstrated that the diversity order is affected by the number of IRS elements and Nakagami- m fading parameters, but the high-SNR slope is not related to these parameters. Simulation results validate our analysis and reveal the superiority of the IRS over the full-duplex decode-and-forward relay.

Index Terms

Intelligent reflecting surface (IRS), non-orthogonal multiple access (NOMA), orthogonal multiple access (OMA).

Part of this work has been submitted to IEEE Global Communications Conference (GLOBECOM) 2020 [1].

Y. Cheng, K. H. Li, and K. C. Teh are with the School of Electrical and Electronic Engineering, Nanyang Technological University, Singapore 639798 (e-mail: ycheng022@e.ntu.edu.sg; ekhli@ntu.edu.sg; ekcteh@ntu.edu.sg).

Y. Liu is with the School of Electronic Engineering and Computer Science, Queen Mary University of London, London E1 4NS, UK (e-mail: yuanwei.liu@qmul.ac.uk).

H. V. Poor is with the Department of Electrical Engineering, Princeton University, Princeton, NJ 08544, USA (e-mail: poor@princeton.edu).

I. INTRODUCTION

Recently, intelligent reflecting surfaces (IRSs) have been proposed as a cost-effective solution to enhance the spectral and energy efficiency of future wireless communication networks [2], [3]. Specifically, an IRS consists of a large number of reconfigurable passive elements, and each element can induce a change of amplitude and phase for the incident signal [4], [5]. By appropriately adjusting amplitude-reflection coefficients and phase-shift variables, it can improve the link quality and enhance the coverage significantly [6]–[8]. Compared with the conventional communication assisting techniques such as relays, the IRS consumes less energy due to passive reflection and is able to operate in full-duplex (FD) mode without self-interference [9].

IRSs have attracted intensive research interest in both academia and industry [10], [11]. In [12], the superiority of an IRS was indicated as compared with a half-duplex (HD) decode-and-forward (DF) relay. In [13], the performance of a system aided by multiple IRSs was evaluated, and it was revealed that the IRS-aided system outperforms the FD DF relay (FDR)-aided system when the number of IRSs exceeds a certain value. Besides wireless communication systems, IRSs can also be applied to optical communication systems. In [14], it was revealed that the outage probability (OP) for an optical communication system can be reduced by introducing an IRS. Passive-beamforming design for IRSs is critical to system performance. In [15], multiple IRSs were deployed in a single-input single-output (SISO) system, and the phase shifts of IRSs were optimized by minimizing the OP. Active and passive beamforming were jointly optimized for IRS-aided multiple-input single-output (MISO) systems in [16]–[18] with different objectives. All aforementioned works assumed the ideal phase-shift model, which is difficult to realize in practice. Hence, the phase shift was assumed to be discrete in [19], and a phase-shift model in which the reflection coefficient is related to the phase shift was proposed in [20]. For physical layer security, IRSs can also enhance system performance by blocking the signals of eavesdroppers [21], [22].

On the other hand, non-orthogonal multiple access (NOMA) has been proposed as a candidate technique for next-generation wireless communication networks as it can improve the spectral efficiency by allocating multiple user devices (UDs) to a single resource block [23], [24]. In [25], the authors presented a fair power allocation algorithm and demonstrated that NOMA always has a larger capacity than orthogonal multiple-access (OMA) under different channel conditions. Allocating many UD to a single carrier is not practical since it leads to high computational

complexity [26]. Hence, UD pairing is a practical solution that can strike a balance between the performance and the computational complexity [27]. In [28], the impact of UD pairing in NOMA systems was investigated, and two UDs with distinct channel conditions were paired to improve system performance. In [29], a two-tier NOMA system was proposed to ensure the distinction of channel conditions for two UDs in a pair.

Since both IRS and NOMA are promising candidate techniques for future wireless communication networks, their combination has been investigated recently [30]–[36]. In [30], an IRS was deployed to improve the coverage by assisting a cell-edge UD in data transmission, where this cell-edge UD is paired with a cell-center UD under the NOMA scheme. The authors further investigated the impact of random phase shifting and coherent phase shifting for an IRS-aided NOMA system in [31]. In [32] and [33], beamforming vectors of the base station (BS) and the IRS were optimized for an IRS-assisted NOMA system. The aforementioned works assumed that the BS-IRS-UD channel is non-line-of-sight (NLoS). Since the IRS can be pre-deployed, the path between the BS and the IRS can be line-of-sight (LoS) [34]–[36]. In [34], the authors assumed the BS-IRS-UD link to be LoS and optimized the active and passive beamforming vectors for a NOMA system aided by an IRS. In [35], the authors studied an IRS-assisted NOMA system by considering ideal and non-ideal IRSs. In [36], the IRS's parameters were designed for a prioritized UD in an IRS-assisted NOMA network.

A. Motivation and Contributions

For IRS-aided NOMA networks, the channel statistics for the BS-IRS-UD link are crucial for the performance evaluation. Most of the existing works have assumed that the BS-IRS-UD link is NLoS, such as [30]–[33]. Some works have assumed that the BS-IRS-UD link is LoS, but without deriving exact channel statistics, e.g., [34]–[36]. This motivates us to consider the BS-IRS-UD link to be either LoS or NLoS, and derive the channel statistics for further analysis. In addition, since the aim of deploying the IRS is to improve the coverage by enhancing the power of cell-edge UDs, we consider a NOMA network in which a cell-edge UD cannot communicate with the BS directly and needs the assistance from an IRS. The cell-edge UD is paired with a cell-center UD to improve system performance [28], [29]. As compared with [1], this paper is more comprehensive, and the contributions can be summarized as follows:

- We study both downlink and uplink transmissions for IRS-aided NOMA and OMA networks.

In particular, we investigate two aspects for each scenario, namely, the OP and the ergodic

rate (ER).

- We adopt the Nakagami- m fading model for the BS-IRS-UD link so that this link can be either LoS or NLoS. Correspondingly, we derive new channel statistics for this link based on the central limit theorem (CLT). Since the CLT-based channel statistics are inaccurate near 0, we further derive exact channel statistics near 0 by utilizing the Laplace transform.
- We derive closed-form expressions for the OP and the ER for each scenario. To gain further insight, we further derive asymptotic approximations of the OP and the ER at a high signal-to-noise ratio (SNR) to obtain the diversity order and the high-SNR slope, respectively. We demonstrate that the number of IRS elements and Nakagami- m fading parameters affect the diversity order but have no influence on the high-SNR slope.
- Finally, we compare the performance of IRS-aided NOMA networks with that of FDR-aided NOMA networks. Simulation results reveal the superiority of the IRS over FDR in the high-SNR regime.

B. Organization and Notation

The remainder of this paper is organized as follows: In Section II, the model of the IRS-aided NOMA network is described. New channel statistics of the BS-IRS-UD link are presented in Section III. The performance analysis for the downlink is conducted in Section IV, followed by the analysis for the uplink in Section V. Furthermore, numerical and simulation results are presented in Section VI. Finally, our conclusions are drawn in Section VII.

In this paper, scalars are denoted by italic letters. Vectors and matrices are denoted by bold-face letters. For a vector \mathbf{v} , $\text{diag}(\mathbf{v})$ denotes a diagonal matrix in which each diagonal element is the corresponding element in \mathbf{v} , respectively. \mathbf{v}^T denotes the transpose of \mathbf{v} . $\arg(\cdot)$ denotes the argument of a complex number. $\mathbb{C}^{x \times y}$ denotes the space of $x \times y$ complex-valued matrices. $P_r(\cdot)$ and $\mathbb{E}(\cdot)$ denote the probability and the expectation, respectively.

II. MODEL OF IRS-AIDED NOMA NETWORKS

We consider an IRS-aided NOMA network with a single-antenna BS and two single-antenna UDs, denoted by N and F, respectively, as shown in Fig. 1. More specifically, N is the cell-center UD that can communicate with the BS directly, while F is the cell-edge UD that needs help from an IRS for communications since there is no direct link between the BS and F due to long distance and blocking objects. The IRS has K reflection elements, and its reflection-coefficient

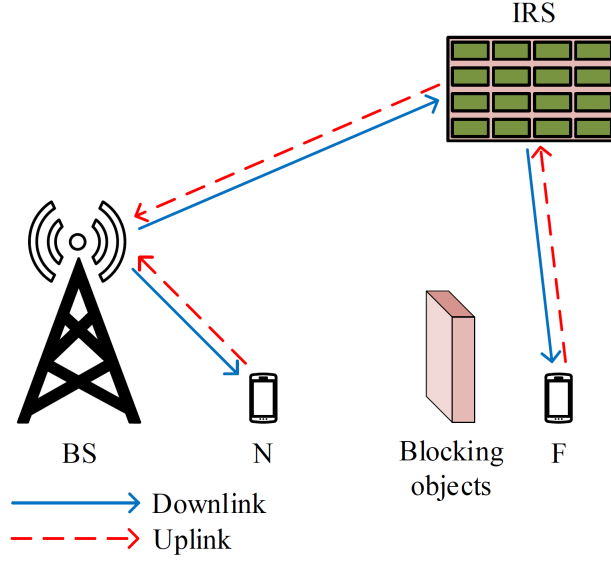


Fig. 1: Model of the IRS-aided NOMA network.

matrix is denoted by $\Theta = \text{diag}(\beta_1 e^{j\theta_1}, \beta_2 e^{j\theta_2}, \dots, \beta_K e^{j\theta_K})$, where $\beta_k \in [0, 1]$ is the amplitude-reflection coefficient and $\theta_k \in [0, 2\pi)$ is the phase-shift variable of the k th element that can be adjusted by the IRS ($k = 1, 2, \dots, K$).

A. Channel Model

All channels experience quasi-static flat fading, and the channel state information (CSI) of all channels is assumed to be perfectly known at the BS. The link between the BS and N is assumed to be NLoS as it is a link between the BS and the ground-UD. Hence, the small-scale fading between the BS and N follows the Rayleigh fading model and is denoted by $h \sim \mathcal{CN}(0, 1)$, where $\mathcal{CN}(\cdot, \cdot)$ is the complex Gaussian distribution. The BS-IRS and IRS-F links can be either LoS or NLoS for different scenarios. Due to the severe path loss, the signals that are reflected by the IRS twice or more times are ignored. The small-scale fading vector between the BS and the IRS is denoted by $\mathbf{G} \in \mathbb{C}^{1 \times K}$. The small-scale fading vector between the IRS and F is denoted by $\mathbf{g} \in \mathbb{C}^{K \times 1}$. Particularly, they are $\mathbf{G} = [G_1, G_2, \dots, G_K]$ and $\mathbf{g} = [g_1, g_2, \dots, g_K]^T$, respectively. All elements in \mathbf{G} and \mathbf{g} follow the Nakagami- m fading model with fading parameters, m_G and m_g , respectively ¹. In particular, it is NLoS for $m_G = 1$ and is LoS for $m_G > 1$ ($\mathcal{G} \in \{G, g\}$).

¹The Nakagami- m fading model and the Rician fading model can be transformed into each other. It obeys the rule of $m = \frac{(K+1)^2}{2K+1}$, where m and K are fading parameters for the Nakagami- m and the Rician models, respectively [37, eq. (3.38)].

B. Signal Model

1) *Downlink*: The BS transmits the signal $x = \sqrt{\alpha_1 P_b} s_1^d + \sqrt{\alpha_2 P_b} s_2^d$, where P_b denotes the transmit power of the BS, s_1^d and s_2^d denote the transmitted signals to N and F, respectively, and α_1 and α_2 denote the power allocation coefficients for N and F, respectively ($\alpha_1 \ll \alpha_2$). The received signals at N and F are given by

$$y_N = h d_N^{-\frac{\alpha_h}{2}} x + n_1, \quad (1)$$

and

$$y_F = \left(\mathbf{G} \Theta \mathbf{g} d_R^{-\frac{\alpha_G}{2}} d_F^{-\frac{\alpha_g}{2}} \right) x + n_2, \quad (2)$$

respectively, where d_N and d_R denote the distances from the BS to N and the IRS, respectively, d_F denotes the distance between the IRS and F, α_h , α_G , and α_g denote the path loss exponents for BS-N, BS-IRS, and IRS-F links, respectively, and n_1 and n_2 denote the additive white Gaussian noises (AWGNs) at N and F, respectively, with the same variance σ_n^2 .

At N, the signal of F is detected first, and the corresponding signal-to-interference-plus-noise ratio (SINR) is given by

$$\text{SINR}_{N,F}^d = \frac{|h|^2 d_N^{-\alpha_h} \alpha_2}{|h|^2 d_N^{-\alpha_h} \alpha_1 + 1/\rho}, \quad (3)$$

where $\rho = P_b/\sigma_n^2$ denotes the transmit SNR of the BS. After implementing the successive interference cancellation (SIC), the signal of N is decoded, and the corresponding SNR is given by

$$\text{SNR}_N^d = |h|^2 d_N^{-\alpha_h} \alpha_1 \rho. \quad (4)$$

At F, its signal is decoded directly by regarding N's signal as interference, and its SINR is given by

$$\text{SINR}_F^d = \frac{|\mathbf{G} \Theta \mathbf{g}|^2 d_R^{-\alpha_G} d_F^{-\alpha_g} \alpha_2}{|\mathbf{G} \Theta \mathbf{g}|^2 d_R^{-\alpha_G} d_F^{-\alpha_g} \alpha_1 + 1/\rho}. \quad (5)$$

Remark 1. For the adaptive-rate transmission, the SINR at F is $\min \{ \text{SINR}_{N,F}^d, \text{SINR}_F^d \}$. However, in the considered system, since F has much more severe path loss than N ($d_N \ll d_F$), we have $\min \{ \text{SINR}_{N,F}^d, \text{SINR}_F^d \} \approx \text{SINR}_F^d$.

2) *Uplink*: The received signal at the BS is given by

$$y = hd_N^{-\frac{\alpha_h}{2}} \sqrt{P_u} s_1^u + \mathbf{G}\Theta\mathbf{g}d_R^{-\frac{\alpha_G}{2}} d_F^{-\frac{\alpha_g}{2}} \sqrt{P_u} s_2^u + n, \quad (6)$$

where P_u denotes the transmit power of each UD, s_1^u and s_2^u denote the transmitted signals from N and F, respectively, and n denotes the AWGN at the BS with variance σ^2 .

At the BS, the signal of N is decoded first by regarding the signal from F as interference, and the corresponding SINR is given by

$$\text{SINR}_N^u = \frac{|h|^2 d_N^{-\alpha_h}}{|\mathbf{G}\Theta\mathbf{g}|^2 d_R^{-\alpha_G} d_F^{-\alpha_g} + 1/\rho'}, \quad (7)$$

where $\rho' = P_u/\sigma^2$ denotes the transmit SNR of each UD. After carrying out the SIC, F's signal is detected with the SNR given by

$$\text{SNR}_F^u = |\mathbf{G}\Theta\mathbf{g}|^2 d_R^{-\alpha_G} d_F^{-\alpha_g} \rho'. \quad (8)$$

III. NEW CHANNEL STATISTICS OF THE BS-IRS-F LINK

In this section, we will present the optimized IRS's parameters and the channel statistics for the BS-IRS-F link.

A. Parameters of the IRS

For the BS-IRS-F link, we aim to provide the best channel quality to F by adjusting parameters of the IRS. That is to maximize $|\mathbf{G}\Theta\mathbf{g}| = \left| \sum_{k=1}^K \beta_k G_k g_k e^{j\theta_k} \right|$ ($j = \sqrt{-1}$), where G_k and g_k are the k th element of \mathbf{G} and \mathbf{g} , respectively. This can be achieved by intelligently adjusting the phase-shift variable θ_k for each element, i.e., the phases of all $G_k g_k e^{j\theta_k}$ are set to be the same. Therefore, there is not only one solution for $\{\theta_k\}$ ($k = 1, 2, \dots, K$), and the generalized solution is given by $\theta_k = \tilde{\theta} - \arg(G_k g_k)$, where $\tilde{\theta}$ is an arbitrary constant ranging in $[0, 2\pi)$. After adopting the optimal $\{\theta_k\}$, we have

$$|\mathbf{G}\Theta\mathbf{g}|^2 = \beta^2 \left(\sum_{k=1}^K |G_k| |g_k| \right)^2, \quad (9)$$

where we assume that $\beta_k = \beta \forall k$ without loss of generality.

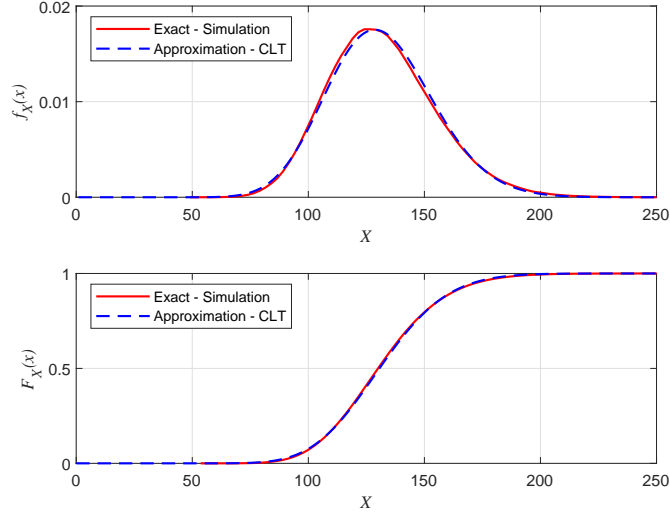


Fig. 2: The PDF and the CDF of X derived by the CLT when $K = 30$, $m_G = 3$, and $m_g = 2$.

B. New Channel Statistics

New channel statistics can be obtained by using the CLT as shown in the following lemma, which has been verified by Monte Carlo simulations as shown in Fig. 2.

Lemma 1. Denote that $X = \frac{(\sum_{k=1}^K |G_k| |g_k|)^2}{K(1-\xi)}$, where $\xi = \frac{1}{m_G m_g} \left(\frac{\Gamma(m_G + \frac{1}{2})}{\Gamma(m_G)} \right)^2 \left(\frac{\Gamma(m_g + \frac{1}{2})}{\Gamma(m_g)} \right)^2$. When the number of IRS elements K is large, X tends to follow a noncentral chi-square distribution as $X \sim \chi_1'^2(\lambda)$, where $\lambda = \frac{K\xi}{1-\xi}$. Its probability density function (PDF) and cumulative distribution function (CDF) are given by

$$f_X(x) = \frac{\lambda^{\frac{1}{4}}}{2} e^{-\frac{x+\lambda}{2}} x^{-\frac{1}{4}} I_{-\frac{1}{2}}(\sqrt{\lambda x}) = e^{-\frac{x+\lambda}{2}} \sum_{i=0}^{\infty} \frac{\lambda^i x^{i-\frac{1}{2}}}{i! 2^{2i+\frac{1}{2}} \Gamma(i + \frac{1}{2})}, \quad (10)$$

for $x \geq 0$ and

$$F_X(x) = 1 - Q_{\frac{1}{2}}(\sqrt{\lambda}, \sqrt{x}) = e^{-\frac{\lambda}{2}} \sum_{i=0}^{\infty} \frac{\lambda^i \gamma(i + \frac{1}{2}, \frac{x}{2})}{i! 2^i \Gamma(i + \frac{1}{2})}, \quad (11)$$

for $x \geq 0$, respectively, where $I_v(\cdot)$ is the modified Bessel function of the first kind, $Q_v(\cdot, \cdot)$ is the Marcum Q -function, $\Gamma(\cdot)$ is the gamma function, and $\gamma(\cdot, \cdot)$ is the lower incomplete gamma function.

Proof. Please refer to Appendix A. ■

Remark 2. The use of CLT results in that $f_X(x)$ is not accurate for $x \rightarrow 0^+$. However, we can still carry out meaningful analysis based on the approximated PDF since it is accurate except in the case of $\int_0^{0^+} g(x)f_X(x)dx$, where $g(x)$ is any function of x .

To address the issue stated in **Remark 2**, we further derive exact channel statistics near 0 without using the CLT as shown in the following lemma.

Lemma 2. Denote that $Z = \sum_{k=1}^K |G_k||g_k|$. When $m_G \neq m_g$, the PDF and the CDF of Z for $z \rightarrow 0^+$ are given by

$$f_Z^{0^+}(z) = \frac{\tilde{m}^K}{\Gamma(2m_s K)} z^{2m_s K - 1} e^{-2\sqrt{m_s m_l} z}, \quad (12)$$

for $z \geq 0$ and

$$F_Z^{0^+}(z) = \frac{\tilde{m}^K (4m_s m_l)^{-m_s K}}{\Gamma(2m_s K)} \gamma(2m_s K, 2\sqrt{m_s m_l} z), \quad (13)$$

for $z \geq 0$, respectively, where $\tilde{m} = \frac{\sqrt{\pi} 4^{m_s - m_l + 1} (m_s m_l)^{m_s} \Gamma(2m_s) \Gamma(2m_l - 2m_s)}{\Gamma(m_s) \Gamma(m_l) \Gamma(m_l - m_s + \frac{1}{2})}$ with $m_s = \min\{m_G, m_g\}$ and $m_l = \max\{m_G, m_g\}$.

Proof. Please refer to Appendix B. ■

IV. PERFORMANCE ANALYSIS FOR DOWNLINK TRANSMISSION

In this section, we will investigate the performance of downlink NOMA and OMA networks. In particular, for each scenario, the OP for the fixed-rate transmission and the ER for the adaptive-rate transmission are derived.

A. NOMA

1) *Outage Probability:* For the fixed-rate transmission system, OP is a widely used metric to measure system performance. The OPs of N and F are given by

$$\mathbb{P}_N^d = 1 - \text{Pr}(\text{SINR}_{N,F}^d \geq \tilde{\gamma}_F, \text{SNR}_N^d \geq \tilde{\gamma}_N), \quad (14)$$

and

$$\mathbb{P}_F^d = \text{Pr}(\text{SINR}_F^d < \tilde{\gamma}_F), \quad (15)$$

respectively, where $\tilde{\gamma}_N = 2^{\tilde{R}_N} - 1$ and $\tilde{\gamma}_F = 2^{\tilde{R}_F} - 1$ with \tilde{R}_N and \tilde{R}_F being the target rates of N and F, respectively. Based on the new channel statistics in **Lemma 1**, the OPs of N and F are derived as shown in the following theorem.

Theorem 1. *In the considered IRS-aided NOMA network, the OPs of N and F for the downlink are given by*

$$\mathbb{P}_N^d = 1 - e^{-\tilde{\rho}_m}, \quad (16)$$

and

$$\mathbb{P}_F^d \approx e^{-\frac{\lambda}{2}} \sum_{i=0}^{\infty} \frac{\lambda^i \gamma \left(i + \frac{1}{2}, \frac{\tilde{\rho}}{2}\right)}{i! 2^i \Gamma\left(i + \frac{1}{2}\right)}, \quad (17)$$

respectively, where $\tilde{\rho}_m = \max\left\{\frac{\tilde{\gamma}_F}{(\alpha_2 - \alpha_1 \tilde{\gamma}_F) a \rho}, \frac{\tilde{\gamma}_N}{a \alpha_1 \rho}\right\}$ and $\tilde{\rho} = \frac{\tilde{\gamma}_F}{(\alpha_2 - \alpha_1 \tilde{\gamma}_F) b \rho}$ with $a = d_N^{-\alpha_h}$ and $b = K \beta^2 (1 - \xi) d_R^{-\alpha_G} d_F^{-\alpha_g}$. Note that when we set power allocation coefficients, we need to ensure that $\alpha_2 - \alpha_1 \tilde{\gamma}_F > 0$.

Proof. First, we denote that $Y = |h|^2$, and its PDF and CDF are given by $f_Y(y) = e^{-y}$ for $y \geq 0$ and $F_Y(y) = 1 - e^{-y}$ for $y \geq 0$, respectively. Then, \mathbb{P}_N^d can be derived as

$$\mathbb{P}_N^d = 1 - \text{Pr}\left(\frac{a \alpha_2 Y}{a \alpha_1 Y + 1/\rho} \geq \tilde{\gamma}_F, a \alpha_1 \rho Y \geq \tilde{\gamma}_N\right) = F_Y(\tilde{\rho}_m). \quad (18)$$

On the other hand, \mathbb{P}_F^d can be derived as

$$\mathbb{P}_F^d = \text{Pr}\left(\frac{b \alpha_2 X}{b \alpha_1 X + 1/\rho} < \tilde{\gamma}_F\right) \approx F_X(\tilde{\rho}). \quad (19)$$

This completes the proof. ■

Remark 3. *According to Remark 2, the OP of F is accurate in the low-SNR regime but is inaccurate in the high-SNR regime. Because the OP of F for $\rho \rightarrow \infty$ is derived by using $\int_0^{0^+} f_X(x) dx$.*

To solve the aforementioned problem, we can use **Lemma 2** to derive the high-SNR approximation of F's OP as shown in the following proposition.

Proposition 1. *In the high-SNR regime, \mathbb{P}_N^d can be approximated as*

$$\mathbb{P}_N^{d,\infty} = \tilde{\rho}_m. \quad (20)$$

When $m_G \neq m_g$, the high-SNR approximation of \mathbb{P}_F^d is given by

$$\mathbb{P}_F^{d,\infty} = \frac{\tilde{m}^K \tilde{c}_1^{2m_s K}}{\Gamma(2m_s K + 1)} \rho^{-m_s K}, \quad (21)$$

where $\tilde{c}_1 = \sqrt{\frac{\tilde{\gamma}_F}{c(\alpha_2 - \alpha_1 \tilde{\gamma}_F)}}$ with $c = \beta^2 d_R^{-\alpha_G} d_F^{-\alpha_g}$.

Proof. By expanding the exponential function in (16) and extracting the leading-order term, we can obtain (20). On the other hand, by expanding the lower incomplete gamma function in (13), we have

$$F_Z^{0+}(z) = \tilde{m}^K \sum_{l=0}^{\infty} \frac{(2\sqrt{m_s m_l})^l z^{l+2m_s K}}{\Gamma(l + 2m_s K + 1)} e^{-2\sqrt{m_s m_l} z}. \quad (22)$$

Then, by using the expansion of the exponential function, we have

$$F_Z^{0+}(z) = \tilde{m}^K \sum_{l=0}^{\infty} \frac{(2\sqrt{m_s m_l})^l z^{l+2m_s K}}{\Gamma(l + 2m_s K + 1)} \sum_{i=0}^{\infty} \frac{(-2\sqrt{m_s m_l})^i z^i}{i!}. \quad (23)$$

Meanwhile, the OP of F for $\rho \rightarrow \infty$ can be derived as

$$\mathbb{P}_F^{d,\infty} = \text{Pr} \left(\frac{c\alpha_2 Z^2}{c\alpha_1 Z^2 + 1/\rho} < \tilde{\gamma}_F \right) = F_Z^{0+} \left(\tilde{c}_1 \rho^{-\frac{1}{2}} \right). \quad (24)$$

Finally, by substituting $z = \tilde{c}_1 \rho^{-\frac{1}{2}}$ into (23) and extracting the leading-order term, we can approximate $\mathbb{P}_F^{d,\infty}$ as (21). This completes the proof. ■

Corollary 1. *In the considered IRS-aided NOMA network, the diversity orders of N and F for the downlink are given by $d_N^d = 1$ and $d_F^d = m_s K$, respectively.*

Proof. Based on **Proposition 1**, we can obtain that the diversity order of F is $m_s K$ when $m_G \neq m_g$. For the case of $m_G = m_g$, it is also $m_s K$ according to the limit. The proof is completed. ■

Remark 4. *The diversity order of F for the downlink NOMA is affected by the number of IRS elements and Nakagami-m fading parameters.*

2) *Ergodic Rate:* For the adaptive-rate transmission system, ER is a commonly used metric to measure system performance. The ERs of N and F are given by

$$R_N^d = \mathbb{E} \left(\log_2 \left(1 + \text{SNR}_N^d \right) \right), \quad (25)$$

and

$$R_F^d = \mathbb{E} \left(\log_2 \left(1 + \text{SINR}_F^d \right) \right), \quad (26)$$

respectively. After some mathematical manipulations, the ERs of N and F are obtained as presented in the following theorem.

Theorem 2. *In the considered IRS-aided NOMA network, the ERs of N and F for the downlink are, respectively, given by*

$$R_N^d = -\frac{e^{\frac{1}{a\alpha_1\rho}}}{\ln(2)} \text{Ei} \left(-\frac{1}{a\alpha_1\rho} \right), \quad (27)$$

and

$$R_F^d \approx \log_2(1 + \tilde{\alpha}) - \frac{e^{-\frac{\lambda}{2}}}{\ln(2)} \sum_{i=0}^{\infty} \frac{\lambda^i}{i! 2^i \Gamma(i + \frac{1}{2})} \sum_{l=1}^{u_1} \omega_{1,l} \mathcal{J}_1(t_l), \quad (28)$$

where $\text{Ei}(\cdot)$ is the exponential integral, $\tilde{\alpha} = \frac{\alpha_2}{\alpha_1}$, $\omega_{1,l} = \frac{\pi}{u_1}$, $t_l = \cos \left(\frac{2l-1}{2u_1} \pi \right)$, and

$$\mathcal{J}_1(t) = \gamma \left(i + \frac{1}{2}, \frac{\tilde{\alpha}(1+t)}{4b\rho\alpha_2 - 2b\rho\alpha_1\tilde{\alpha}(1+t)} \right) \frac{\sqrt{1-t^2}}{1 + \frac{2}{\tilde{\alpha}} + t}. \quad (29)$$

Proof. Please refer to Appendix C. ■

Remark 5. *The ER of F is accurate as the calculation is not related to $\int_0^{0+} g(x) f_X(x) dx$. Because of the principle of downlink NOMA, the ER of N increases for the increase of the SNR, while the ER of F approaches a ceiling when $\rho \rightarrow \infty$.*

To provide insight into the performance, the high-SNR slope is considered that is defined as $S = \lim_{\rho \rightarrow \infty} \frac{R(\rho)}{\log_2(\rho)}$ [38]. To obtain it, the asymptotic expression for N's ER and the ceiling for F's ER are derived in the following proposition.

Proposition 2. *In the high-SNR regime, R_N^d can be approximated as*

$$R_N^{d,\infty} = \log_2(a\alpha_1\rho) - \frac{E_c}{\ln(2)}, \quad (30)$$

where E_c denotes the Euler constant. On the other hand, the ceiling for R_F^d in the high-SNR regime is given by

$$R_F^{d,\infty} = \log_2(1 + \tilde{\alpha}). \quad (31)$$

Proof. By using $\lim_{x \rightarrow 0} e^x = 1$ and $\text{Ei}(-x) \approx \ln(x) + E_c$ for $x \rightarrow 0$ [39, eq. (8.214.2)], we can approximate (27) as (30) when $\rho \rightarrow \infty$. On the other hand, since we have $\lim_{\rho \rightarrow \infty} \frac{b\alpha_2 X}{b\alpha_1 X + 1/\rho} = \tilde{\alpha}$, we can approximate (26) as (31) when $\rho \rightarrow \infty$. This completes the proof. ■

Corollary 2. *In the considered IRS-aided NOMA network, the high-SNR slopes of N and F for the downlink are given by $S_N^d = 1$ and $S_F^d = 0$, respectively.*

Proof. We have $S_N^d = \frac{dR_N^{d,\infty}}{d \log_2(\rho)} = \ln(2)\rho \frac{dR_N^{d,\infty}}{d\rho} = 1$, and this completes the proof. ■

Remark 6. *The high-SNR slope of F for the downlink NOMA is not related to the number of IRS elements and Nakagami-m fading parameters.*

B. OMA

OMA can be regarded as a special case of NOMA. The data rates of N and F under the OMA scheme are given by $\frac{1}{2} \log_2(1 + |h|^2 d_N^{-\alpha_h} \rho)$ and $\frac{1}{2} \log_2\left(1 + \beta^2 \left(\sum_{k=1}^K |G_k| |g_k|\right)^2 d_R^{-\alpha_G} d_F^{-\alpha_g} \rho\right)$, respectively. Here, we assume that each UD share half of the resource block.

1) *Outage Probability:* The OPs of N and F for the downlink are presented in the following theorem.

Theorem 3. *When N and F are under the downlink OMA scheme, their OPs are given by*

$$\mathbb{P}_N^{do} = 1 - e^{-\frac{\tilde{\gamma}_N^o}{a\rho}}, \quad (32)$$

and

$$\mathbb{P}_F^{do} \approx e^{-\frac{\lambda}{2}} \sum_{i=0}^{\infty} \frac{\lambda^i \gamma\left(i + \frac{1}{2}, \frac{\tilde{\gamma}_F^o}{2b\rho}\right)}{i! 2^i \Gamma\left(i + \frac{1}{2}\right)}, \quad (33)$$

respectively, where $\tilde{\gamma}_N^o = 2^{2\tilde{R}_N} - 1$ and $\tilde{\gamma}_F^o = 2^{2\tilde{R}_F} - 1$.

Proof. \mathbb{P}_N^{do} and \mathbb{P}_F^{do} can be derived as follows:

$$\mathbb{P}_N^{do} = \text{Pr}(a\rho Y < \tilde{\gamma}_N^o) = F_Y\left(\frac{\tilde{\gamma}_N^o}{a\rho}\right), \quad (34)$$

and

$$\mathbb{P}_F^{do} = \text{Pr}(b\rho X < \tilde{\gamma}_F^o) \approx F_X\left(\frac{\tilde{\gamma}_F^o}{b\rho}\right). \quad (35)$$

This completes the proof. ■

Remark 7. According to **Remark 2**, \mathbb{P}_F^{do} is accurate in the low-SNR regime but is inaccurate in the high-SNR regime. Because \mathbb{P}_F^{do} for $\rho \rightarrow \infty$ is derived by using $\int_0^{0+} f_X(x)dx$.

To address the problem in **Remark 7**, we use **Lemma 2** and obtain the high-SNR approximation of \mathbb{P}_F^{do} that is shown in the following proposition.

Proposition 3. In the high-SNR regime, \mathbb{P}_N^{do} can be approximated as

$$\mathbb{P}_N^{do,\infty} = \frac{\tilde{\gamma}_N^o}{a} \rho^{-1}. \quad (36)$$

When $m_G \neq m_g$, the high-SNR approximation of \mathbb{P}_F^{do} is given by

$$\mathbb{P}_F^{do,\infty} = \frac{\tilde{m}^K \tilde{c}_2^{2m_s K}}{\Gamma(2m_s K + 1)} \rho^{-m_s K}, \quad (37)$$

where $\tilde{c}_2 = \sqrt{\frac{\tilde{\gamma}_F^o}{c}}$.

Proof. Similar to the proof of **Proposition 1**. ■

Corollary 3. When N and F are under the downlink OMA scheme, the diversity orders of N and F are given by $d_N^{do} = 1$ and $d_F^{do} = m_s K$, respectively.

Remark 8. The diversity order of F for the downlink OMA is affected by the number of IRS elements and Nakagami- m fading parameters. Moreover, the diversity orders of N and F for the downlink OMA are the same as these for the downlink NOMA, respectively.

2) *Ergodic Rate:* The ERs of N and F for OMA are presented in the following theorem.

Theorem 4. When N and F are under the downlink OMA scheme, their ERs are, respectively, given by

$$R_N^{do} = -\frac{e^{\frac{1}{a\rho}}}{2 \ln(2)} \text{Ei} \left(-\frac{1}{a\rho} \right), \quad (38)$$

and

$$R_F^{do} \approx \frac{\lambda^{\frac{1}{4}}}{4} e^{-\frac{\lambda}{2}} \sum_{l=1}^{u_2} \omega_{2,l} \mathcal{J}_2(x_{2,l}), \quad (39)$$

where $x_{2,l}$ is the l th root of Laguerre polynomial $L_{u_2}(x)$, $\omega_{2,l} = \frac{x_{2,l}}{(u_2+1)^2 (L_{u_2+1}(x_{2,l}))^2}$, and

$$\mathcal{J}_2(x) = x^{-\frac{1}{4}} e^{\frac{x}{2}} \log_2(1 + b\rho x) I_{-\frac{1}{2}} \left(\sqrt{\lambda x} \right). \quad (40)$$

Proof. For N, the analysis is similar to the proof of **Theorem 2**. For the ER of F, it can be expressed as

$$R_F^{do} \approx \int_0^\infty \frac{1}{2} \log_2(1 + b\rho x) f_X(x) dx = \frac{\lambda^{\frac{1}{4}}}{4} e^{-\frac{\lambda}{2}} \underbrace{\int_0^\infty x^{-\frac{1}{4}} e^{-\frac{x}{2}} \log_2(1 + b\rho x) I_{-\frac{1}{2}}(\sqrt{\lambda x}) dx}_{J_2}. \quad (41)$$

Next, J_2 can be approximated by using the Gauss-Laguerre quadrature. As such, we have

$$J_2 \simeq \sum_{l=1}^{w_2} \omega_{2,l} \mathcal{J}_2(x_{2,l}). \quad (42)$$

This completes the proof. ■

Remark 9. *The ER of F is accurate as the calculation is not related to $\int_0^{0+} g(x) f_X(x) dx$. On the other hand, both ERs of N and F increase as the SNR increases.*

Then, the approximations in the high-SNR regime are given in the following proposition.

Proposition 4. *In the high-SNR regime, the approximations of R_N^{do} and R_F^{do} are given by*

$$R_N^{do,\infty} = \frac{1}{2} \left(\log_2(a\rho) - \frac{E_c}{\ln(2)} \right), \quad (43)$$

and

$$R_F^{do,\infty} = \frac{1}{2} \log_2(1 + b\rho(1 + \lambda)), \quad (44)$$

respectively.

Proof. For N, the analysis is similar to the proof of **Proposition 2**. For F, we have $\mathbb{E}(X) = 1 + \lambda$ according to the property of the noncentral chi-square distribution. Then, since $\frac{1}{2} \log_2(1 + b\rho X)$ with respect to X is concave, with the aid of the Jensen's inequality [40], we have

$$R_F^{do} = \mathbb{E} \left(\frac{1}{2} \log_2(1 + b\rho X) \right) \leq \frac{1}{2} \log_2(1 + b\rho \mathbb{E}(X)) = \frac{1}{2} \log_2(1 + b\rho(1 + \lambda)). \quad (45)$$

When $\rho \rightarrow \infty$, R_F^{do} can be approximated as (44), and the proof is completed. ■

Corollary 4. *When N and F are under the downlink OMA scheme, their high-SNR slopes are given by $S_N^{do} = 0.5$ and $S_F^{do} = 0.5$, respectively.*

Proof. Similar to the proof of **Corollary 2**. ■

Remark 10. *The high-SNR slope of N for the downlink OMA is half of that for the downlink NOMA. On the other hand, the high-SNR slope of F in downlink OMA networks, which is not related to the number of IRS elements and Nakagami- m fading parameters, is larger than that in downlink NOMA networks.*

V. PERFORMANCE ANALYSIS FOR UPLINK TRANSMISSION

In this section, we will investigate the performance of the uplink transmission. The analyses of OP and ER will be presented in the following.

A. NOMA

1) *Outage Probability:* The OPs of N and F are, respectively, given by

$$\mathbb{P}_N^u = \text{Pr}(\text{SINR}_N^u < \tilde{\gamma}_N), \quad (46)$$

and

$$\mathbb{P}_F^u = 1 - \text{Pr}(\text{SINR}_N^u \geq \tilde{\gamma}_N, \text{SNR}_F^u \geq \tilde{\gamma}_F). \quad (47)$$

Then, the closed-form expressions for OPs can be derived, and the results are shown in the following theorem.

Theorem 5. *In the considered IRS-aided NOMA network, the OPs of N and F for the uplink are given by*

$$\mathbb{P}_N^u \approx 1 - e^{-\frac{\tilde{\gamma}_N}{a\rho'} - \frac{\lambda}{2}} \sum_{i=0}^{\infty} \frac{\lambda^i}{i! 2^{2i+\frac{1}{2}} \left(\frac{b\tilde{\gamma}_N}{a} + \frac{1}{2}\right)^{i+\frac{1}{2}}}, \quad (48)$$

and

$$\mathbb{P}_F^u \approx 1 - e^{-\frac{\tilde{\gamma}_N}{a\rho'} - \frac{\lambda}{2}} \sum_{i=0}^{\infty} \frac{\lambda^i \Gamma\left(i + \frac{1}{2}, \frac{\tilde{\gamma}_N \tilde{\gamma}_F}{a\rho'} + \frac{\tilde{\gamma}_F}{2b\rho'}\right)}{i! 2^{2i+\frac{1}{2}} \left(\frac{b\tilde{\gamma}_N}{a} + \frac{1}{2}\right)^{i+\frac{1}{2}} \Gamma\left(i + \frac{1}{2}\right)}, \quad (49)$$

respectively, where $\Gamma(\cdot, \cdot)$ is the upper incomplete gamma function.

Proof. The OP of N can be transformed into

$$\begin{aligned} \mathbb{P}_N^u &= \text{Pr}\left(\frac{aY}{bX + 1/\rho'} < \tilde{\gamma}_N\right) \approx \int_0^\infty \int_0^{\frac{b\tilde{\gamma}_N x}{a} + \frac{\tilde{\gamma}_N}{a\rho'}} f_Y(y) dy f_X(x) dx \\ &= 1 - e^{-\frac{\tilde{\gamma}_N}{a\rho'} - \frac{\lambda}{2}} \sum_{i=0}^{\infty} \frac{\lambda^i}{i! 2^{2i+\frac{1}{2}} \Gamma\left(i + \frac{1}{2}\right)} \int_0^\infty e^{-\left(\frac{b\tilde{\gamma}_N}{a} + \frac{1}{2}\right)x} x^{i-\frac{1}{2}} dx. \end{aligned} \quad (50)$$

Furthermore, by referring to [39, eq. (3.381.4)], (48) can be derived. Similarly, the OP of F can be first transformed into

$$\begin{aligned}\mathbb{P}_F^u &= 1 - \text{Pr} \left(\frac{aY}{bX + 1/\rho'} \geq \tilde{\gamma}_N, b\rho' X \geq \tilde{\gamma}_F \right) \approx 1 - \int_{\frac{\tilde{\gamma}_F}{b\rho'}}^{\infty} \int_{\frac{b\tilde{\gamma}_N x + \tilde{\gamma}_N}{a}}^{\infty} f_Y(y) dy f_X(x) dx \\ &= 1 - e^{-\frac{\tilde{\gamma}_N}{a\rho'} - \frac{\lambda}{2}} \sum_{i=0}^{\infty} \frac{\lambda^i}{i! 2^{2i+\frac{1}{2}} \Gamma(i+\frac{1}{2})} \int_{\frac{\tilde{\gamma}_F}{b\rho'}}^{\infty} e^{-\left(\frac{b\tilde{\gamma}_N}{a} + \frac{1}{2}\right)x} x^{i-\frac{1}{2}} dx.\end{aligned}\quad (51)$$

Then, by referring to [39, eq. (3.381.3)], we can derive the closed-form expression as (49). This completes the proof. \blacksquare

Remark 11. *The OP of N is accurate since it does not involve the integral of $\int_0^{0+} g(x) f_X(x) dx$. Although the calculation of F's OP is related to $\int_0^{0+} g(x) f_X(x) dx$, it only has a small bias in the medium-SNR regime. This is because F's OP must be higher than N's OP and converges to a floor in the high-SNR regime with N's OP due to the principle of uplink NOMA.*

The floor for OPs of both UDs is presented in the following proposition.

Proposition 5. *In the high-SNR regime, \mathbb{P}_N^u and \mathbb{P}_F^u approach the same floor as*

$$\mathbb{P}_{both}^{u,\infty} = 1 - e^{-\frac{\lambda}{2}} \sum_{i=0}^{\infty} \frac{(\lambda)^i}{i! 2^{2i+\frac{1}{2}} \left(\frac{b\tilde{\gamma}_N}{a} + \frac{1}{2}\right)^{i+\frac{1}{2}}}.\quad (52)$$

Proof. We have that $\lim_{\rho' \rightarrow \infty} e^{-\frac{\tilde{\gamma}_N}{a\rho'}} = 1$ and $\lim_{\rho' \rightarrow \infty} \Gamma\left(i + \frac{1}{2}, \frac{\tilde{\gamma}_N \tilde{\gamma}_F}{a\rho'} + \frac{\tilde{\gamma}_F}{2b\rho'}\right) = \Gamma\left(i + \frac{1}{2}\right)$. Thus, the limit of both \mathbb{P}_N^u and \mathbb{P}_F^u for $\rho' \rightarrow \infty$ can be obtained, and the proof is completed. \blacksquare

Corollary 5. *In the considered IRS-aided NOMA network, both diversity orders of N and F for the uplink are 0, i.e., $d_N^u = 0$ and $d_F^u = 0$.*

Remark 12. *The diversity order of F for the uplink NOMA is not related to the number of IRS elements and Nakagami-m fading parameters.*

2) *Ergodic Rate:* The ERs of the N and F are given by

$$R_N^u = \mathbb{E}(\log_2(1 + \text{SINR}_N^u)),\quad (53)$$

and

$$R_F^u = \mathbb{E}(\log_2(1 + \text{SNR}_F^u)),\quad (54)$$

respectively. Then, the ERs of N and F can be obtained, and the results are provided in the following theorem.

Theorem 6. *In the considered IRS-aided NOMA network, the ER of N for the uplink is given by*

$$R_N^u \approx -\frac{\lambda^{\frac{1}{4}}}{2 \ln(2)} e^{\frac{1}{a\rho'} - \frac{\lambda}{2}} \sum_{l=1}^{u_3} \omega_{3,l} \mathcal{J}_3(x_{3,l}), \quad (55)$$

where $x_{3,l}$ is the l th root of Laguerre polynomial $L_{u_3}(x)$, $\omega_{3,l} = \frac{x_{3,l}}{(u_3+1)^2 (L_{u_3+1}(x_{3,l}))^2}$ is the weight, and

$$\mathcal{J}_3(x) = x^{-\frac{1}{4}} e^{(\frac{b}{a} + \frac{1}{2})x} \text{Ei} \left(-\frac{b}{a}x - \frac{1}{a\rho'} \right) I_{-\frac{1}{2}} \left(\sqrt{\lambda x} \right). \quad (56)$$

On the other hand, the ER of F for the uplink is given by

$$R_F^u \approx \frac{\lambda^{\frac{1}{4}}}{2} e^{-\frac{\lambda}{2}} \sum_{l=1}^{u_4} \omega_{4,l} \mathcal{J}_4(x_{4,l}), \quad (57)$$

where $x_{4,l}$ is the l th root of Laguerre polynomial $L_{u_4}(x)$, $\omega_{4,l} = \frac{x_{4,l}}{(u_4+1)^2 (L_{u_4+1}(x_{4,l}))^2}$, and

$$\mathcal{J}_4(x) = x^{-\frac{1}{4}} e^{\frac{x}{2}} \log_2 \left(1 + b\rho'x \right) I_{-\frac{1}{2}} \left(\sqrt{\lambda x} \right). \quad (58)$$

Proof. Please refer to Appendix D. ■

Remark 13. *Both ERs are accurate as they are not related to the integral of $\int_0^{0+} g(x) f_X(x) dx$. Due to the principle of uplink NOMA, the ER of N approaches a ceiling when $\rho' \rightarrow \infty$, while the ER of F increases as the SNR increases.*

The ceiling for N and the high-SNR approximation for F are presented in the following proposition.

Proposition 6. *In the high-SNR regime, R_N^u approaches a ceiling that is given by*

$$R_N^{u,\infty} \approx -\frac{\lambda^{\frac{1}{4}}}{2 \ln(2)} e^{-\frac{\lambda}{2}} \sum_{l=1}^{u_3} \omega_{3,l} \mathcal{J}_3^\infty(x_{3,l}), \quad (59)$$

where

$$\mathcal{J}_3^\infty(x) = x^{-\frac{1}{4}} e^{(\frac{b}{a} + \frac{1}{2})x} \text{Ei} \left(-\frac{b}{a}x \right) I_{-\frac{1}{2}} \left(\sqrt{\lambda x} \right). \quad (60)$$

On the other hand, the high-SNR approximation of R_F^u is given by

$$R_F^{u,\infty} = \log_2 \left(1 + b\rho'(1 + \lambda) \right). \quad (61)$$

Proof. For N, when $\rho' \rightarrow \infty$, we have $\frac{1}{a\rho'} \rightarrow 0$. Hence, based on (55) and (56), we can obtain (59). For F, the analysis is similar to the proof of **Proposition 4**. ■

Corollary 6. *In the considered IRS-aided NOMA network, the high-SNR slopes of N and F for the uplink are given by $S_N^u = 0$ and $S_F^u = 1$, respectively.*

Proof. Similar to the proof of **Corollary 2**. ■

Remark 14. *The high-SNR slope of F for the uplink NOMA is not affected by the number of IRS elements and Nakagami- m fading parameters.*

B. OMA

For OMA, the performance analyses for the uplink and the downlink are similar, and we can obtain all results for the uplink by referring to Section IV-B in a simple method, i.e., replacing the transmit SNR of the BS (ρ) by the transmit SNR of the UD (ρ').

After completing all analyses for downlink and uplink networks, all results related to diversity order and high-SNR slope are summarized in Table I for ease of reference.

TABLE I: Diversity order and high-SNR slope for each scenario

Multiple-access scheme	UD	Downlink		Uplink	
		d	S	d	S
NOMA	N	1	1	0	0
	F	$m_s K$	0	0	1
OMA	N	1	0.5	1	0.5
	F	$m_s K$	0.5	$m_s K$	0.5

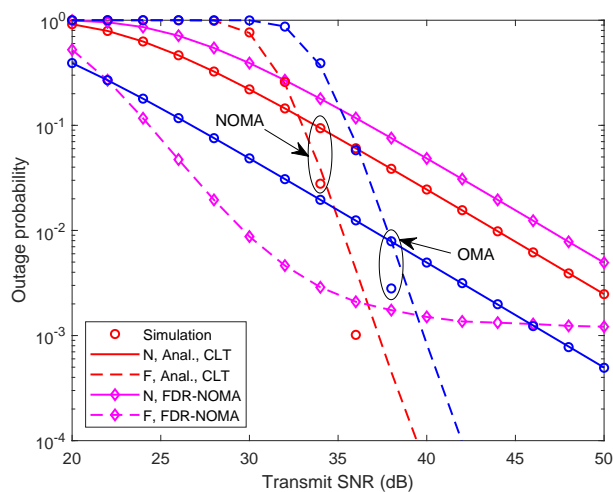
VI. NUMERICAL RESULTS AND DISCUSSION

In this section, numerical results are presented for the performance evaluation of the considered network. Meanwhile, Monte Carlo simulations are conducted to verify the accuracy. The parameters are shown in Table II.

For comparisons, we regard an FDR-aided NOMA network as the benchmark. Specifically, an FDR under the classic protocol is deployed at the place of the IRS to help F to communicate with the BS. The FDR works under a realistic assumption that is the same as [41]. Specifically, the self-interference channel is denoted by h_r , and follows $\mathcal{CN}(0, \lambda_r)$. Since the reflection at the

TABLE II: Parameters setting

Bandwidth	$B = 1$ MHz
Amplitude-reflection coefficient of the IRS	$\beta = 0.9$
Distances	$d_N = 20$ m, $d_R = 80$ m, and $d_F = 20$ m
Path-loss exponents	$\alpha_h = 3.5$, $\alpha_G = 2.5$, and $\alpha_g = 2.5$
Nakagami- m fading parameters	$m_G = 3$ and $m_g = 1.5$
Target data-rates for the fixed-rate transmission	$\tilde{R}_N = \tilde{R}_F = 1$ Kbps
Power-allocation coefficients for the downlink	$\alpha_1 = 0.1$ and $\alpha_2 = 0.9$
Number of points for Chebyshev-Gauss and Gauss-Laguerre quadratures	$u_1 = u_2 = u_3 = u_4 = 100$

Fig. 3: OPs versus the transmit SNR in downlink networks when $K = 10$.

IRS is passive without consuming the energy, for fairness, we assume that the transmit power at the BS and the FDR is $P_b^r = 0.5P_b$ for the downlink, and the transmit power at F and the FDR is $P_u^r = 0.5P_u$ for the uplink.

A. Downlink Networks

In Fig. 3, the OPs versus the transmit SNR in IRS-aided NOMA, IRS-aided OMA, and FDR-aided NOMA networks of downlink are plotted. First, the analyses of N for both NOMA and OMA are accurate as all simulation results coincide with the corresponding analytical results that are derived from (16) and (32). For F, the analyses under these two schemes that are derived from (17) and (33) are accurate in the low-SNR regime but are inaccurate in the high-SNR

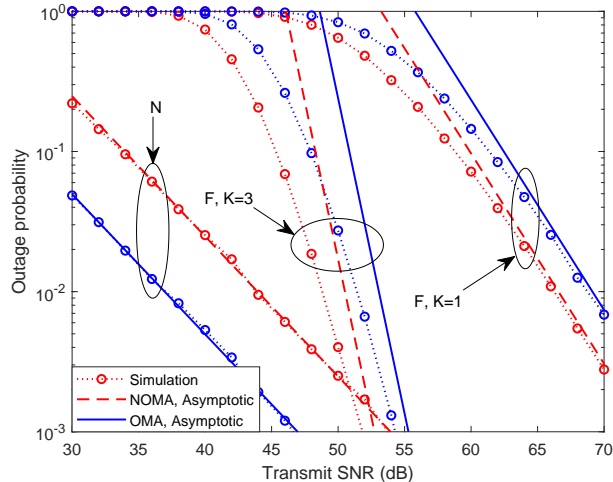


Fig. 4: High-SNR approximations of OPs in downlink networks when $K = 1$ and $K = 3$.

regime, which results from the use of the CLT-based channel statistics. As a benchmark, the OP curves for the FDR-aided system are plotted for comparisons. We observe that N in the IRS-aided NOMA system always has better performance than that in the FDR-aided NOMA system, since the transmit power of the BS in the former system is twice that in the latter. For F, the FDR-aided system has better performance than the IRS-aided system in the low-SNR regime, since the IRS transmission experiences severe path loss, which has been pointed out in [31]. Nevertheless, in the high-SNR regime, the IRS-aided system has much better performance. One reason is that the OP of F in the FDR-aided system converges to a floor in the high-SNR regime due to the self-interference. On the other hand, F in the IRS-aided system has a large diversity order, which is the advantage of the IRS over the FDR.

In Fig. 4, we plot the high-SNR approximate curves when $K = 1$ and $K = 3$. We observe that the OPs of N and F for NOMA and OMA gradually approach their respective asymptotic curves derived from (20), (21), (36), and (37), which validates our analysis. Furthermore, by observing slopes, both diversity orders of N under NOMA and OMA schemes are 1 when $K = 1$ and $K = 3$ since the value of K has no influence on the OP of N. For F, the diversity orders under these two schemes are the same. They are equal to 1.5 and 4.5 for $K = 1$ and $K = 3$, respectively, which is consistent with **Corollary 1** and **Corollary 3**.

In Fig. 5, the ER curves for different downlink networks are depicted. First, it is observed that the simulation points for IRS-aided NOMA and OMA networks match well with the

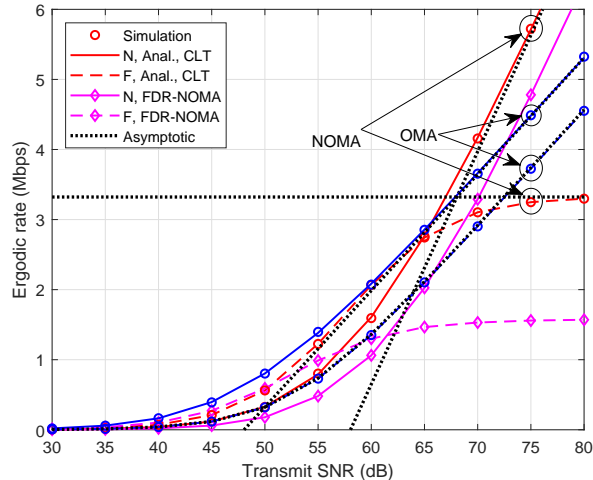


Fig. 5: ERs versus the transmit SNR in downlink networks when $K = 30$.

corresponding analytical results that are derived from (27), (28), (38), and (39). It is also observed that the high-SNR approximations that are derived from (30), (31), (43), and (44) are accurate, and hence, it can be used to derive high-SNR slopes. We observe that the high-SNR slope of N for NOMA is 1^2 , while that for OMA is 0.5. Due to the principle of downlink NOMA, the ER of F approaches a ceiling in the high-SNR regime, while that under the OMA scheme has a high-SNR slope of 0.5, which coincides with **Corollary 2** and **Corollary 4**. As a benchmark, the ER curves of the FDR-aided NOMA are plotted for comparisons. It is observed that N in the IRS-aided system always has a higher ER than that in the FDR-aided system, since the transmit power of the BS in the former system is twice that in the latter. On the other hand, for F, the ER in the IRS-aided system is lower than that in the FDR-aided system in the low-SNR regime. This is because the IRS transmission experience severe path loss, which has been pointed out in [31]. As the SNR increases, the ER of F in the IRS-aided system approaches a higher ceiling than that in the FDR-aided system due to the existence of the self-interference channel when using the FDR, which demonstrates the superiority of IRS again.

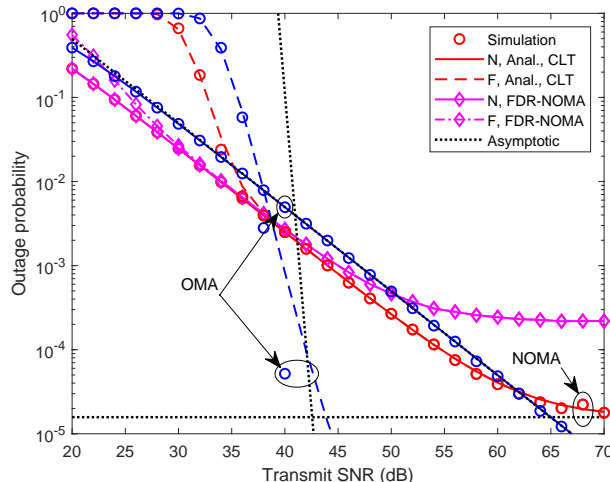


Fig. 6: OPs versus the transmit SNR in uplink networks when $K = 10$.

B. Uplink Networks

In Fig. 6, the OPs versus the transmit SNR in different uplink networks are plotted. For the IRS-aided NOMA network, it is observed that the simulation points of N match well with the analytical results that are derived from (48). The simulation results of F have a small bias with the analytical results from (49) in the medium-SNR regime, which is consistent with our explanation in **Remark 11**. Then, we observe that both OPs of N and F decrease as the increase of the transmit SNR and approach a floor gradually that is derived from (52). This is because of the principle of uplink NOMA that F's signal is regarded as interference to decode N's signal. Thus, the diversity orders of both UDs are 0, which is consistent with **Corollary 5**. For OMA, since there is no interference, the OPs of both UDs decrease as the transmit SNR increases. The diversity orders of N and F are 1 and 15, respectively, by observing the slopes of asymptotic curves. Finally, it is observed that the OPs for the FDR-aided NOMA network also approach a floor. In Fig. 6, the floor for the IRS-aided network is lower than that for the FDR-aided network. However, the former will be higher than the latter if we increase K . Thus, for uplink IRS-aided networks, the contribution of the IRS to OP is not obvious.

In Fig. 7, the ER curves for different uplink networks are depicted. For the IRS-aided NOMA network, we observe that the simulated results coincide with the corresponding analytical results

²The high-SNR slope of 1 corresponds to the slope of $0.1 \log_2 10 \approx 0.33$ in Fig. 5.

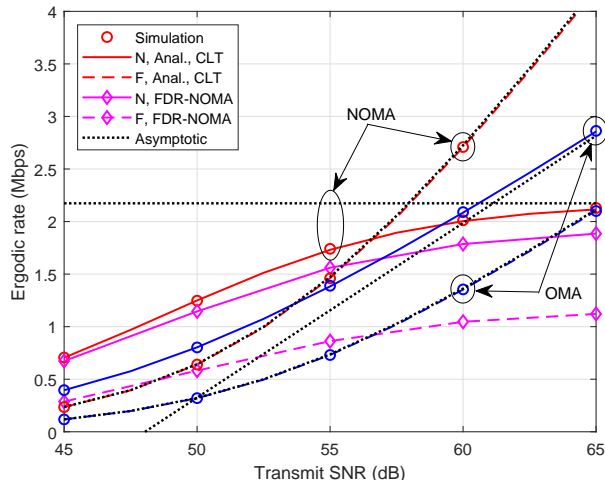


Fig. 7: ERs versus the transmit SNR in uplink networks when $K = 30$.

that are derived from (55) and (57). In addition, the approximations in the high-SNR regime that are derived from (59) and (61) are also asymptotic exact. Following that, it is observed that the high-SNR slopes of N and F are 0 and 1, respectively, which is consistent with **Corollary 6**. It is also observed that both UDs have the same high-SNR slope of 0.5 under the OMA scheme. Lastly, we observe that N in the FDR-aided NOMA network also converges to a ceiling. For F, it remains increasing with the increase of the transmit SNR in the IRS-aided network, while it has a ceiling in the FDR-aided network due to the self-interference, revealing the advantage of the IRS.

VII. CONCLUSIONS

In this paper, we have studied IRS-aided NOMA and OMA networks for downlink and uplink transmissions. With the derivation of new channel statistics, closed-form expressions for the OP and the ER have been derived. Furthermore, the diversity order and the high-SNR slope for each scenario have been obtained to provide insight into the performance. It has been demonstrated that the diversity order is related to the number of IRS elements and Nakagami- m fading parameters, while the high-SNR slope is not affected by these parameters. Since this work focuses on SISO networks, IRS-aided MISO networks are worthy of investigation for future work.

APPENDIX A
PROOF OF LEMMA 1

Based on the property of the Nakagami- m fading model, the expectation and variance of $|\mathcal{G}_k|$ are $\mu_{\mathcal{G}} = \left(\frac{1}{m_{\mathcal{G}}}\right)^{\frac{1}{2}} \frac{\Gamma(m_{\mathcal{G}} + \frac{1}{2})}{\Gamma(m_{\mathcal{G}})}$ and $\text{Var}_{\mathcal{G}} = 1 - \frac{1}{m_{\mathcal{G}}} \left(\frac{\Gamma(m_{\mathcal{G}} + \frac{1}{2})}{\Gamma(m_{\mathcal{G}})}\right)^2$, respectively, where $\mathcal{G} \in \{G, g\}$. Then, the expectation and variance of $|G_k||g_k|$ are $\mu_p = \mu_g \mu_G = \sqrt{\xi}$ and $\text{Var}_p = (\text{Var}_g + \mu_g^2)(\text{Var}_G + \mu_G^2) - \mu_g^2 \mu_G^2 = 1 - \xi$, respectively. Next, since all $|G_k||g_k|$ ($k = 1, 2, \dots, K$) are independent and identically distributed (i.i.d.), based on the CLT, $\sum_{k=1}^K |G_k||g_k|$ tends towards a Gaussian distribution as

$$\sum_{k=1}^K |G_k||g_k| \sim \mathcal{N}(K\mu_p, K\text{Var}_p). \quad (\text{A.1})$$

Furthermore, we unify the variance and have

$$\frac{\sum_{k=1}^K |G_k||g_k|}{\sqrt{K\text{Var}_p}} \sim \mathcal{N}\left(\frac{\sqrt{K}\mu_p}{\sqrt{\text{Var}_p}}, 1\right). \quad (\text{A.2})$$

Hence, $X = \frac{(\sum_{k=1}^K |G_k||g_k|)^2}{K\text{Var}_p}$ follows a noncentral chi-square distribution $\chi_1'^2(\lambda)$ with a PDF given by

$$f_X(x) = \frac{\lambda^{\frac{1}{4}}}{2} e^{-\frac{x+\lambda}{2}} x^{-\frac{1}{4}} I_{-\frac{1}{2}}(\sqrt{\lambda x}), \quad (\text{A.3})$$

where $\lambda = \frac{K\mu_p^2}{\text{Var}_p}$ and

$$I_{-\frac{1}{2}}(\sqrt{\lambda x}) = \left(\frac{\sqrt{\lambda x}}{2}\right)^{-\frac{1}{2}} \sum_{i=0}^{\infty} \frac{\left(\frac{\lambda x}{4}\right)^i}{i! \Gamma(i + \frac{1}{2})}. \quad (\text{A.4})$$

The CDF of X is given by

$$F_X(x) = 1 - Q_{\frac{1}{2}}(\sqrt{\lambda}, \sqrt{x}), \quad (\text{A.5})$$

where

$$Q_{\frac{1}{2}}(\sqrt{\lambda}, \sqrt{x}) = 1 - e^{-\frac{\lambda}{2}} \sum_{i=0}^{\infty} \left(\frac{\lambda}{2}\right)^i \frac{\gamma\left(i + \frac{1}{2}, \frac{x}{2}\right)}{i! \Gamma\left(i + \frac{1}{2}\right)}. \quad (\text{A.6})$$

This completes the proof.

APPENDIX B
PROOF OF LEMMA 2

Denote that $Q_k = |G_k||g_k|$. According to [42], the PDF of Q_k (the product of two Nakagami- m random variables) is given by

$$f_{Q_k}(q) = \frac{4(m_s m_l)^{\frac{m_s+m_l}{2}}}{\Gamma(m_s)\Gamma(m_l)} q^{m_s+m_l-1} K_{m_s-m_l}(2\sqrt{m_s m_l}q), \quad (\text{B.1})$$

for $q \geq 0$, where $K_v(\cdot)$ is the modified Bessel function of the second kind. The Laplace transform of f_{Q_k} is derived as

$$\mathcal{L}_{f_{Q_k}}(s) = \frac{4(m_s m_l)^{\frac{m_s+m_l}{2}}}{\Gamma(m_s)\Gamma(m_l)} \int_0^\infty q^{m_s+m_l-1} e^{-sq} K_{m_s-m_l}(2\sqrt{m_s m_l}q) dq. \quad (\text{B.2})$$

Furthermore, by referring to [39, eq. (6.621.3)], we have

$$\mathcal{L}_{f_{Q_k}}(s) = \phi (s + 2\sqrt{m_s m_l})^{-2m_s} F\left(2m_s, m_s - m_l + \frac{1}{2}; m_s + m_l + \frac{1}{2}; \frac{s - 2\sqrt{m_s m_l}}{s + 2\sqrt{m_s m_l}}\right), \quad (\text{B.3})$$

where $\phi = \frac{\sqrt{\pi} 4^{m_s-m_l+1} (m_s m_l)^{m_s} \Gamma(2m_s) \Gamma(2m_l)}{\Gamma(m_s) \Gamma(m_l) \Gamma(m_s+m_l+\frac{1}{2})}$ and $F(\cdot, \cdot; \cdot; \cdot)$ is the hypergeometric series. When $s \rightarrow \infty$, since $m_s < m_l$ satisfies the condition of [39, eq. (9.122.1)], we have

$$\mathcal{L}_{f_{Q_k}}^\infty(s) = \tilde{m} (s + 2\sqrt{m_s m_l})^{-2m_s}. \quad (\text{B.4})$$

Since all Q_k ($k = 1, 2, \dots, K$) are i.i.d., the Laplace transform of the PDF of $Z = \sum_{k=1}^K Q_k$ for $s \rightarrow \infty$ is given by

$$\mathcal{L}_{f_Z}^\infty(s) = \prod_{k=1}^K \mathcal{L}_{f_{Q_k}}^\infty(s) = \tilde{m}^K (s + 2\sqrt{m_s m_l})^{-2m_s K}. \quad (\text{B.5})$$

Thus, by conducting the inverse Laplace transform for (B.5), the PDF of Z for $z \rightarrow 0^+$ can be derived as (12) based on [39, eq. (17.13.3)]. Following that, according to [39, eq. (3.351.1)], the CDF of Z for $z \rightarrow 0^+$ can be derived as (13). This completes the proof.

APPENDIX C
PROOF OF THEOREM 2

First, we have

$$R_N^d = - \int_0^\infty \log_2(1 + a\alpha_1 \rho y) d(1 - F_Y(y)) = \frac{1}{\ln(2)} \int_0^\infty \frac{e^{-y}}{y + \frac{1}{a\alpha_1 \rho}} dy. \quad (\text{C.1})$$

Then, by referring to [39, eq. (3.352.4)], we can derive (27). To obtain R_F^d , we denote that $\tilde{X} = \frac{b\alpha_2 X}{b\alpha_1 X + 1/\rho}$, and the corresponding CDF is given by

$$F_{\tilde{X}}(\tilde{x}) = F_X\left(\frac{\tilde{x}}{b\rho(\alpha_2 - \tilde{x}\alpha_1)}\right) = e^{-\frac{\lambda}{2}} \sum_{i=0}^{\infty} \frac{\lambda^i \gamma\left(i + \frac{1}{2}, \frac{\tilde{x}}{2b\rho(\alpha_2 - \tilde{x}\alpha_1)}\right)}{i! 2^i \Gamma\left(i + \frac{1}{2}\right)}. \quad (\text{C.2})$$

Hence, we have

$$\begin{aligned} R_F^d &\approx - \int_0^{\tilde{\alpha}} \log_2(1 + \tilde{x}) d(1 - F_{\tilde{X}}(\tilde{x})) = \frac{1}{\ln(2)} \int_0^{\tilde{\alpha}} \frac{1 - F_{\tilde{X}}(\tilde{x})}{1 + \tilde{x}} d\tilde{x} \\ &= \log_2(1 + \tilde{\alpha}) - \frac{1}{\ln(2)} e^{-\frac{\lambda}{2}} \sum_{i=0}^{\infty} \frac{\lambda^i}{i! 2^i \Gamma\left(i + \frac{1}{2}\right)} \underbrace{\int_0^{\tilde{\alpha}} \frac{\gamma\left(i + \frac{1}{2}, \frac{\tilde{x}}{2b\rho(\alpha_2 - \tilde{x}\alpha_1)}\right)}{1 + \tilde{x}} d\tilde{x}}_{J_1}, \end{aligned} \quad (\text{C.3})$$

where $\tilde{\alpha} = \frac{\alpha_2}{\alpha_1}$. To further transform J_1 , we denote that $t = \frac{2\tilde{x}}{\alpha} - 1$. Then, we have

$$J_1 = \int_{-1}^1 \frac{\gamma\left(i + \frac{1}{2}, \frac{\tilde{\alpha}(1+t)}{2b\rho(2\alpha_2 - \alpha_1\tilde{\alpha}(1+t))}\right)}{1 + \frac{2}{\alpha} + t} dt. \quad (\text{C.4})$$

Next, by using the Chebyshev-Gauss quadrature, we can approximate J_1 as

$$J_1 \simeq \sum_{l=1}^{u_1} \omega_{1,l} \mathcal{J}_1(t_l). \quad (\text{C.5})$$

This completes the proof.

APPENDIX D

PROOF OF THEOREM 6

First, the ER of N can be transformed into

$$\begin{aligned} R_N^u &\approx \int_0^{\infty} \left(- \int_0^{\infty} \log_2\left(1 + \frac{ay}{bx + 1/\rho}\right) d(1 - F_Y(y)) \right) f_X(x) dx \\ &= \frac{1}{\ln(2)} \int_0^{\infty} \left(\int_0^{\infty} \frac{e^{-y}}{y + \frac{b}{a}x + \frac{1}{a\rho}} dy \right) f_X(x) dx. \end{aligned} \quad (\text{D.1})$$

Then, by referring to [39, eq. (3.352.4)], (D.1) can be rewritten as

$$\begin{aligned} R_N^u &\approx - \frac{1}{\ln(2)} \int_0^{\infty} e^{\frac{b}{a}x + \frac{1}{a\rho}} \text{Ei}\left(-\left(\frac{b}{a}x + \frac{1}{a\rho}\right)\right) f_X(x) dx \\ &= - \frac{\lambda^{\frac{1}{4}}}{2 \ln(2)} e^{\frac{1}{a\rho} - \frac{\lambda}{2}} \underbrace{\int_0^{\infty} x^{-\frac{1}{4}} e^{(\frac{b}{a} - \frac{1}{2})x} \text{Ei}\left(-\frac{b}{a}x - \frac{1}{a\rho}\right) I_{-\frac{1}{2}}(\sqrt{\lambda x}) dx}_{J_3}. \end{aligned} \quad (\text{D.2})$$

Next, by using the Gauss-Laguerre quadrature, we have

$$J_3 \simeq \sum_{l=1}^{u_3} \omega_{3,l} \mathcal{J}_3(x_{3,l}). \quad (\text{D.3})$$

For the ER of F, it can be expressed as

$$R_F^u \approx \int_0^\infty \log_2(1 + b\rho x) f_X(x) dx = \frac{\lambda^{\frac{1}{4}}}{2} e^{-\frac{\lambda}{2}} \underbrace{\int_0^\infty x^{-\frac{1}{4}} e^{-\frac{x}{2}} \log_2(1 + b\rho x) I_{-\frac{1}{2}}(\sqrt{\lambda x}) dx}_{J_4}. \quad (\text{D.4})$$

Next, J_4 also can be approximated by adopting the Gauss-Laguerre quadrature. As such, we have

$$J_4 \simeq \sum_{l=1}^{u_4} \omega_{4,l} \mathcal{J}_4(x_{4,l}). \quad (\text{D.5})$$

This completes the proof.

REFERENCES

- [1] Y. Cheng, K. H. Li, Y. Liu, and K. C. Teh, "Outage performance of downlink IRS-assisted NOMA systems," in *Proc. IEEE Global Communications Conference (GLOBECOM) 2020*, Submitted for publication.
- [2] Z. Wang, L. Liu, and S. Cui, "Channel estimation for intelligent reflecting surface assisted multiuser communications: Framework, algorithms, and analysis," [Online]. Available: <https://arxiv.org/abs/1912.11783>.
- [3] M. Cui, G. Zhang, and R. Zhang, "Secure wireless communication via intelligent reflecting surface," *IEEE Wireless Commun. Lett.*, vol. 8, no. 5, pp. 1410–1414, Oct. 2019.
- [4] B. Ning, Z. Chen, W. Chen, Y. Du, and J. Fang, "Channel estimation and hybrid beamforming for reconfigurable intelligent surfaces assisted THz communications," [Online]. Available: <https://arxiv.org/abs/1912.11662>.
- [5] H. Shen, W. Xu, S. Gong, Z. He, and C. Zhao, "Secrecy rate maximization for intelligent reflecting surface assisted multi-antenna communications," *IEEE Commun. Lett.*, vol. 23, no. 9, pp. 1488–1492, Sep. 2019.
- [6] G. Zhou, C. Pan, H. Ren, K. Wang, and A. Nallanathan, "A framework of robust transmission design for IRS-aided MISO communications with imperfect cascaded channels," [Online]. Available: <https://arxiv.org/abs/2001.07054>.
- [7] L. Dong and H.-M. Wang, "Secure MIMO transmission via intelligent reflecting surface," *IEEE Wireless Commun. Lett.*, to be published.
- [8] K. Feng, Q. Wang, X. Li, and C.-K. Wen, "Deep reinforcement learning based intelligent reflecting surface optimization for MISO communication systems," *IEEE Wireless Commun. Lett.*, to be published.
- [9] Q. Wu and R. Zhang, "Towards smart and reconfigurable environment: Intelligent reflecting surface aided wireless network," [Online]. Available: <https://arxiv.org/abs/1905.00152>.
- [10] W. Shi, X. Zhou, L. Jia, Y. Wu, F. Shu, and J. Wang, "Enhanced secure wireless information and power transfer via intelligent reflecting surface," [Online]. Available: <https://arxiv.org/abs/1911.01001>.
- [11] Ö. Özdogan, E. Björnson, and E. G. Larsson, "Intelligent reflecting surfaces: Physics, propagation, and pathloss modeling," *IEEE Wireless Commun. Lett.*, to be published.
- [12] E. Björnson, Ö. Özdogan, and E. G. Larsson, "Intelligent reflecting surface versus decode-and-forward: How large surfaces are needed to beat relaying?" *IEEE Wireless Commun. Lett.*, vol. 9, no. 2, pp. 244–248, Feb. 2020.
- [13] J. Lyu and R. Zhang, "Spatial throughput characterization for intelligent reflecting surface aided multiuser system," [Online]. Available: <https://arxiv.org/abs/2001.02447>.
- [14] H. Wang, Z. Zhang, B. Zhu, J. Dang, L. Wu, L. Wang, K. Zhang, and Y. Zhang, "Performance of wireless optical communication with reconfigurable intelligent surfaces and random obstacles," [Online]. Available: <https://arxiv.org/abs/2001.05715>.

- [15] Z. Zhang, Y. Cui, F. Yang, and L. Ding, "Analysis and optimization of outage probability in multi-intelligent reflecting surface-assisted systems," [Online]. Available: <https://arxiv.org/abs/1909.02193>.
- [16] X. Yu, D. Xu, and R. Schober, "MISO wireless communication systems via intelligent reflecting surfaces," in *Proc. IEEE/CIC International Conference on Communications in China (ICCC)*, Changchun, China, Aug. 2019, pp. 735–740.
- [17] Q. Wu and R. Zhang, "Intelligent reflecting surface enhanced wireless network via joint active and passive beamforming," *IEEE Trans. Wireless Commun.*, vol. 18, no. 11, pp. 5394–5409, Nov. 2019.
- [18] H. Guo, Y.-C. Liang, J. Chen, and E. G. Larsson, "Weighted sum-rate optimization for intelligent reflecting surface enhanced wireless networks," [Online]. Available: <https://arxiv.org/abs/1905.07920>.
- [19] C. You, B. Zheng, and R. Zhang, "Progressive channel estimation and passive beamforming for intelligent reflecting surface with discrete phase shifts," [Online]. Available: <https://arxiv.org/abs/1912.10646>.
- [20] S. Abeywickrama, R. Zhang, and C. Yuen, "Intelligent reflecting surface: Practical phase shift model and beamforming optimization," [Online]. Available: <https://arxiv.org/abs/1907.06002>.
- [21] H. Han, J. Zhao, D. Niyato, M. Di Renzo, and Q.-V. Pham, "Intelligent reflecting surface aided network: Power control for physical-layer broadcasting," [Online]. Available: <https://arxiv.org/abs/1910.14383>.
- [22] X. Guan, Q. Wu, and R. Zhang, "Intelligent reflecting surface assisted secrecy communication via joint beamforming and jamming," [Online]. Available: <https://arxiv.org/abs/1907.12839>.
- [23] Y. Liu, H. Xing, C. Pan, A. Nallanathan, M. Elkashlan, and L. Hanzo, "Multiple-antenna-assisted non-orthogonal multiple access," *IEEE Wireless Commun.*, vol. 25, no. 2, pp. 17–23, Apr. 2018.
- [24] Y. Cheng, K. H. Li, K. C. Teh, S. Luo, and W. Wang, "Performance analysis of cooperative NOMA systems with adaptive mode selection and subchannel allocation," *IEEE Trans. Veh. Technol.*, vol. 68, no. 11, pp. 10 981–10 990, Nov. 2019.
- [25] J. A. Oviedo and H. R. Sadjadpour, "A fair power allocation approach to NOMA in multi-user SISO systems," *IEEE Trans. Veh. Technol.*, vol. 66, no. 9, pp. 7974–7985, Sep. 2017.
- [26] Y. Cheng, K. H. Li, K. C. Teh, S. Luo, and W. Wang, "Two-step user pairing for OFDM-based cooperative NOMA systems," *IEEE Commun. Lett.*, vol. 24, no. 4, pp. 903–906, Apr. 2020.
- [27] Y. Liu, Z. Qin, M. Elkashlan, Y. Gao, and L. Hanzo, "Enhancing the physical layer security of non-orthogonal multiple access in large-scale networks," *IEEE Trans. Wireless Commun.*, vol. 16, no. 3, pp. 1656–1672, Mar. 2017.
- [28] Z. Ding, P. Fan, and H. V. Poor, "Impact of user pairing on 5G nonorthogonal multiple-access downlink transmissions," *IEEE Trans. Veh. Technol.*, vol. 65, no. 8, pp. 6010–6023, Aug. 2016.
- [29] Y. Liu, Z. Ding, M. Elkashlan, and H. V. Poor, "Cooperative non-orthogonal multiple access with simultaneous wireless information and power transfer," *IEEE J. Sel. Areas Commun.*, vol. 34, no. 4, pp. 938–953, Apr. 2016.
- [30] Z. Ding and H. V. Poor, "A simple design of IRS-NOMA transmission," [Online]. Available: <https://arxiv.org/abs/1907.09918>.
- [31] Z. Ding, R. Schober, and H. V. Poor, "On the impact of phase shifting designs on IRS-NOMA," *IEEE Wireless Commun. Lett.*, to be published.
- [32] J. Zhu, Y. Huang, J. Wang, K. Navaie, and Z. Ding, "Power efficient IRS-assisted NOMA," [Online]. Available: <https://arxiv.org/abs/1912.11768>.
- [33] M. Fu, Y. Zhou, and Y. Shi, "Intelligent reflecting surface for downlink non-orthogonal multiple access networks," [Online]. Available: <https://arxiv.org/abs/1906.09434>.
- [34] G. Yang, X. Xu, and Y.-C. Liang, "Intelligent reflecting surface assisted non-orthogonal multiple access," [Online]. Available: <https://arxiv.org/abs/1907.03133>.
- [35] X. Mu, Y. Liu, L. Guo, J. Lin, and N. Al-Dhahir, "Exploiting intelligent reflecting surfaces in multi-antenna aided NOMA systems," [Online]. Available: <https://arxiv.org/abs/1910.13636>.

- [36] T. Hou, Y. Liu, Z. Song, X. Sun, Y. Chen, and L. Hanzo, "Reconfigurable intelligent surface aided NOMA networks," [Online]. Available: <https://arxiv.org/abs/1912.10044>.
- [37] A. Goldsmith, *Wireless Communications*, 1st ed. Cambridge, UK: Cambridge university press, 2005.
- [38] A. Lozano, A. M. Tulino, and S. Verdú, "High-SNR power offset in multiantenna communication," *IEEE Trans. Inf. Theory*, vol. 51, no. 12, pp. 4134–4151, Dec. 2005.
- [39] I. S. Gradshteyn and I. M. Ryzhik, *Table of Integrals, Series, and Products*, 7th ed. Amsterdam, The Netherlands: Elsevier, 2007.
- [40] Y. Liu, Z. Qin, M. Elkashlan, A. Nallanathan, and J. A. McCann, "Non-orthogonal multiple access in large-scale heterogeneous networks," *IEEE J. Sel. Areas Commun.*, vol. 35, no. 12, pp. 2667–2680, Dec. 2017.
- [41] C. Zhong and Z. Zhang, "Non-orthogonal multiple access with cooperative full-duplex relaying," *IEEE Commun. Lett.*, vol. 20, no. 12, pp. 2478–2481, Dec. 2016.
- [42] N. Bhargav, C. R. N. da Silva, Y. J. Chun, É. J. Leonardo, S. L. Cotton, and M. D. Yacoub, "On the product of two κ - μ random variables and its application to double and composite fading channels," *IEEE Trans. Wireless Commun.*, vol. 17, no. 4, pp. 2457–2470, Apr. 2018.